Simplified Numerical Model of an Axial Impeller

Andrei-Mugur Georgescu[1], and Sanda-Carmen Georgescu[*2]
[1]Hydraulics and Environmental Protection Department, Technical University of Civil Engineering Bucharest, [2]Hydraulics and Hydraulic Machinery Department, University "Politehnica" of Bucharest
*Corresponding author: 313 Spl. Independentei, 060042, Bucharest, Romania, carmen.georgescu@upb.ro

Abstract: We propose a simplified numerical method to model the flow field downstream of an axial impeller, a method that can be used for any axial hydraulic machinery for which, one is less interested by the actual flow between the blades, than by the flow field downstream of the hydraulic machinery. The proposed method is applied here to an axial fan for which, in the studied configuration, pressure - flow rate curve is available from the literature. Numerical results are obtained using COMSOL Multiphysics' 3D turbulent incompressible flow built on a Reynolds average formulation of Navier-Stokes equations, with *k-ε* closure. Our computed results are in good agreement with measured or computed values of the flow downstream of such a hydraulic machinery. The method has proven to save a lot of computational time.

Keywords: axial impeller, axial fan, axial hydraulic machinery, volume force coefficients.

1. Introduction

Our aim is to simulate the flow field downstream of an axial impeller, using a simplified numerical method. "Simplified method" means that one doesn't have to model the actual blades of the axial hydraulic machinery and use a rotating mesh to numerically calculate the flow field downstream of the machinery, but rather to insert some force coefficients in a subdomain representing the impeller, which will produce on the flow the same average effects as the blades of the impeller.

There are many applications to such a "simplified method". Suppose we want to numerically model air cooling in a desktop computer, we would have to model at least the cooler fan and the source fan to get the correct flow field. This would be computational resources and time consuming if done using the actual geometry of the impeller and a rotating mesh algorithm. With the simplified proposed method we only have to define the subdomains of the impellers and add inside those domains some force coefficients and define some integration variables. This was just a trivial example, but there are other significant applications like forced coolers, cooling towers, drying kilns and all sorts of axial mixers for liquid solutions. This method could also be applied (with an inverse sign for the variable force coefficients) to model axial wind turbines farms or axial marine current turbines farms, where the interaction and most efficient arrangement of the turbines in the farm are of major importance.

In this paper, the selected study case is an experimental unit equipped with an axial fan (Figure 1), namely the FM41 unit designed by Armfield, from the Hydraulics Laboratory of Technical University of Civil Engineering Bucharest.

Figure 1. FM41 Axial Fan Demonstration Unit.

For the axial fan placed in this configuration, we know the rotational speed of the fan, $n = 45$ rot/s, and its pressure Δp - flow rate Q curve; those are the only data we need for our simplified numerical method. The $\Delta p = \Delta p(Q)$ curve is expressed as a second order polynomial regression curve that fits experimental data (Figure 2), namely:

$$\Delta p = c_0 - c_2 Q^2 = 60 - 42000\, Q^2 \qquad (1)$$

where the pressure Δp is in Pa, and the airflow rate Q is in m^3/s. If the studied hydraulic machinery is an axial pump or an axial turbine, the operation curve will be the head H - flow rate Q curve, which can be expressed as a third or second order polynomial regression curve.

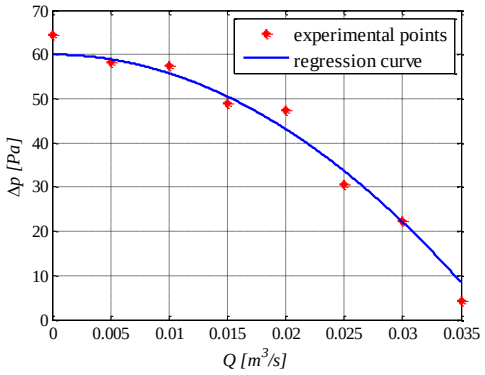

Figure 2. Operation curve of the studied axial fan.

As already mentioned, we are interested by the flow field downstream of the studied axial fan, and our computed results for the velocity distribution across a flow section (e.g. the outlet section at the end of the discharge duct) can be compared with measured velocity profile in the same section. Our numerical model ignore the calibrated orifice plate, which is used within the FM41 unit near the fan discharge, to measure the airflow rate.

2. Use of COMSOL Multiphysics

Numerical simulations are performed for the 3D turbulent incompressible flow built on a Reynolds Averaged Navier-Stokes (RANS) calculation, using the $k-\varepsilon$ turbulence model.

As mentioned before, instead of modeling the blades of the axial fan, we need to insert volume force coefficients in a subdomain of b length representing the impeller (Figure 3), and to define integration variable giving Q at the inlet of the impeller for each iteration. The above force coefficients are attached to volume forces F_x, F_y, F_z in the body forces fields of the Navier-Stokes equations, being variable with the flow rate Q, as:

$$F_x = \frac{\Delta p}{b} = \frac{60 - 42000Q^2}{0.04}, \qquad (2)$$

$$F_y = \frac{-\Delta p^2 z\,|z|}{7675\left(y^2+z^2\right)^2}, \qquad (3)$$

$$F_z = \frac{\Delta p^2 y\,|y|}{7675\left(y^2+z^2\right)^2}, \qquad (4)$$

where all forces are in N/m^3, being divided by impeller's length (for our model, $b = 0.04$ m). The coefficient equal to 7675 from equations (3) and (4) represents the term $8\pi^2\rho n^2 b$, derived from the y and z components of the tangential velocity of the fluid within the impeller; here, the air density is $\rho = 1.2$ kg/m^3 and fan's rotational speed is $n = 45$ rot/s. So, as it will be proven, the above force coefficients will produce on the downstream flow the same average effects as impeller's blades.

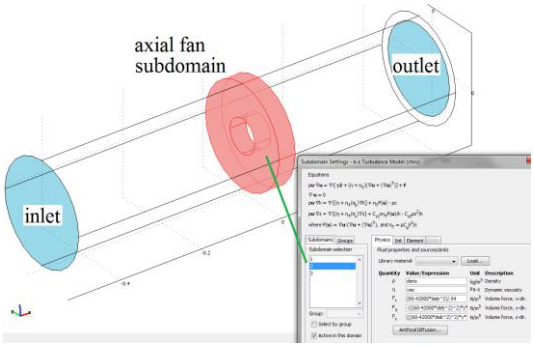

Figure 3. Axial fan subdomain, where we insert the volume force coefficients.

The geometry of the studied model (a model built at the same scale as the FM41 experimental unit) is presented in Figure 4.

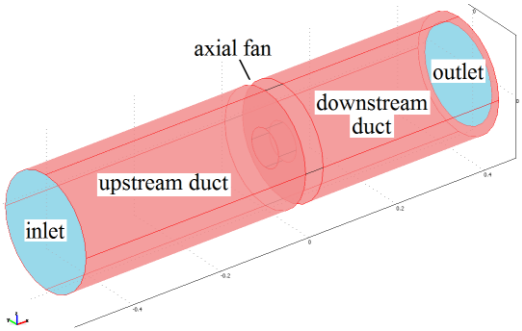

Figure 4. Computational flow domain.

We imposed the following boundary conditions: atmospheric pressure (meaning 0 differential pressure), no viscous stress, on both inlet and outlet sections (Figure 4), and logarithmic wall function, with $h/2$ wall offset, on model's walls, namely on the cylindrical walls of the upstream and downstream ducts; the outer and inner cylindrical walls of the impeller subdomain (enclosing the space usually occupied

by impeller's blades); the annular disc wall at the outlet section, which diminishes the outlet section area with respect to the inlet section area.

The 3D computational mesh for the studied model is presented in Figure 5, and consists of 4158 tetrahedral elements, 1200 triangular boundary elements, 172 edge elements, and 28 vertex elements, yielding 33406 degrees of freedom, with 0.0014 element volume ratio.

The mesh quality is presented in Figure 6; it is characterized by 0.3364 minimum element quality.

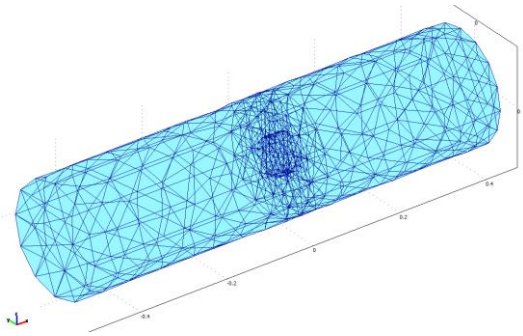

Figure 5. Computational mesh.

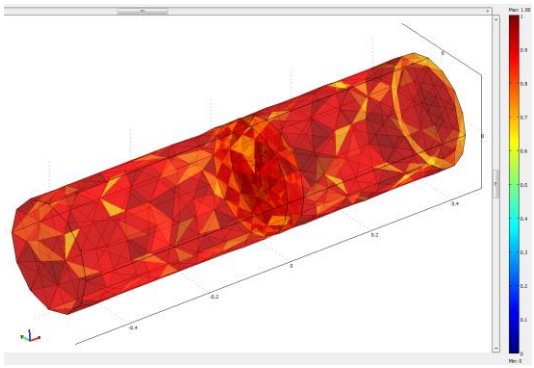

Figure 6. Mesh quality.

3. Numerical Results

In this section we present some results obtained for the numerical simulation of the airflow in the studied rectilinear configuration, consisting of an upstream duct, a fictitious impeller of an axial fan (which presence is replaced by volume force coefficients), and a downstream duct.

The velocity field and the pressure field, as *xOz* slices and *xOy* slices, before and downstream the axial fan, are presented in Figures 7 and 8. Some isosurfaces of the velocity field are presented in Figure 9.

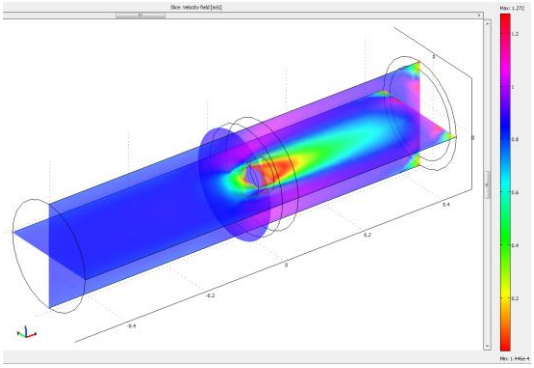

Figure 7. Velocity field along the studied model.

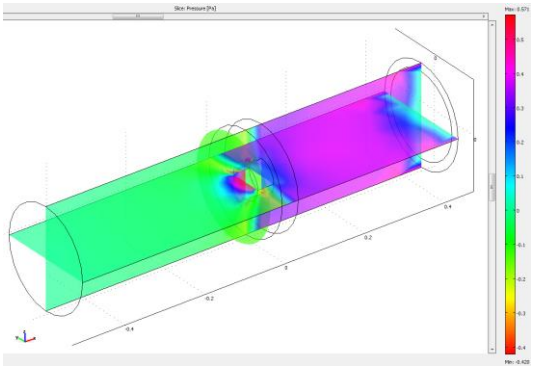

Figure 8. Pressure field along the studied model.

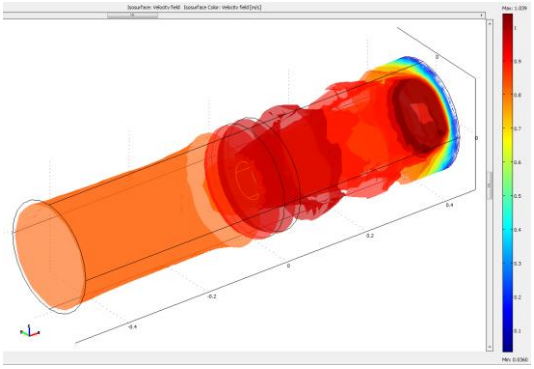

Figure 9. Isosurfaces of the velocity field.

Further, we present the evolution of the vorticity along the studied model, from the regular distribution with weak values near the inlet section (Figure 10), to slightly increasing values and irregular distribution just before the impeller (Figure 11), to high values inside the impeller subdomain, especially near impeller's hub (Figure 12), and finally to slightly smaller

values and quite regular distribution at the exit section (Figure 13).

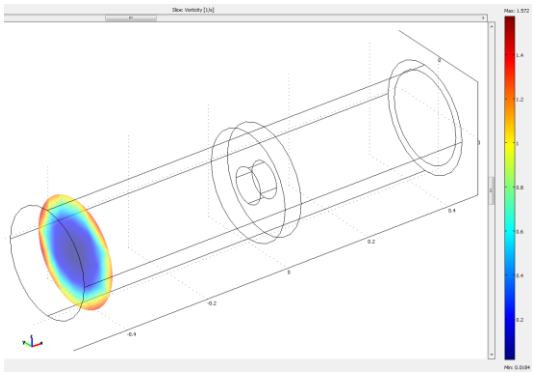

Figure 10. Vorticity distribution near the inlet.

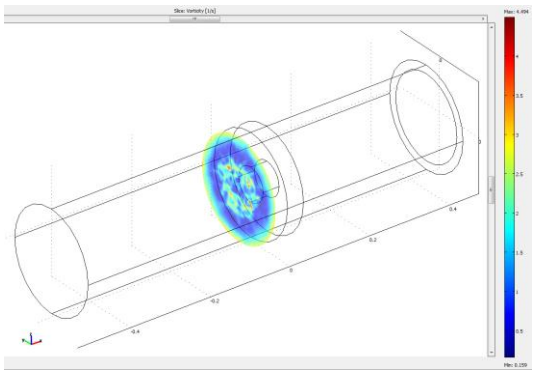

Figure 11. Vorticity just before the impeller.

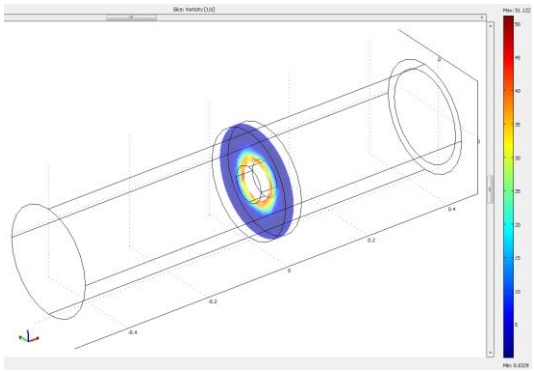

Figure 12. Vorticity inside the impeller subdomain.

4. Conclusions

Our computed results are found to be in good agreement with measured or computed values of the flow downstream of the studied axial fan, attached to the experimental unit FM41. The method has proven to save a lot of computational time, e.g. a computation took less than 18 minutes on a workstation with 16GB memory and 2 quad-core Intel Xeon 2.66GHz processors.

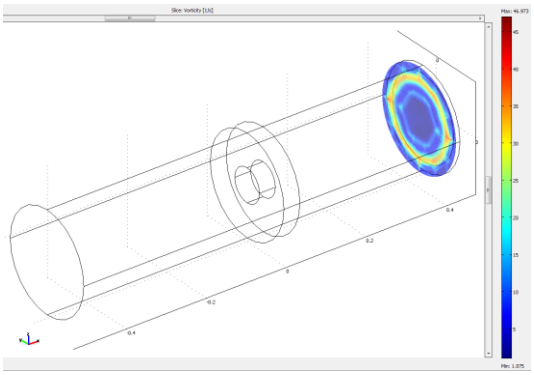

Figure 13. Vorticity distribution at the exit.

5. References

1. J. R. Bredell, D. G. Kröger, G. D. Thiart, Numerical investigation into aerodynamic blade loading in large axial flow fans operating under distorted inflow conditions, *R & D Journal*, **22**(2), 11-17 (2006)
2. C. J. Meyer, D. G. Kröger, A numerical investigation of the errors associated with the scaling of axial flow fan performance characteristics, *R & D Journal*, **20**(2), 16-24 (2004)
3. F. N. le Roux, *The CFD simulation of an axial flow fan*, 14-60, 76, 85, 105, 113. MSc Thesis, University of Stellenbosch, South Africa (2010)
4. S. J. van der Spuy, T. W. von Backström, Performance of rotor-only axial fans designed for minimum exit kinetic energy, *R & D Journal*, **18**(3), 63-69 (2002)
5. S. J. van der Spuy, T. W. von Backström, D. G. Kröger, An evaluation of simplified methods to model the performance of axial flow fan arrays, *R & D Journal of the South African Institution of Mechanical Engineering*, **26**, 12-20 (2010)